JMEPEG (2025) 34:25946–25953
https://doi.org/10.1007/s11665-025-11725-1

1059-9495/$19.00

ORIGINAL RESEARCH ARTICLE

Effects of Strain and Inter-Pass Time on the Restoration Behavior of 436 Stainless Steels

Muhammed Salojee, Charles W. Siyasiya, Kofi A. Annan, and Joseph S. Moema

Submitted: 29 October 2024 / Revised: 23 April 2025 / Accepted: 7 June 2025 / Published online: 18 August 2025

Ferritic stainless steels (FSSs) are viable alternatives to nickel containing austenitic stainless steels. The AISI 436 FSS grade is fully ferritic at all temperature ranges, and therefore, grain refinement can only be achieved through controlling inclusions during solidification and/or recrystallization. In this work, the effects of strain and inter-pass time on the restoration behavior of 436 were systematically investigated using the Gleeble 1500 thermomechanical processing simulator. The aim of the study was to promote the accumulation of strain by delaying recrystallization during roughing rolling simulation to improve the driving force for recrystallization during finishing rolling simulation at lower temperature. Three roughing rolling schedules were designed, i.e., the first simulated the existing industry practice (Control), the second with increased inter-pass time (INT) and the last with both increased inter-pass time and strain per pass (INT + S). Roughing and finishing were each simulated in three-passes, amounting to a total of six-passes. The SEM-EBSD results revealed that the Control and INT schedules resulted in higher strain localization, particularly around particles. On the contrary, the increased inter-pass times and strains (INT + S) led to less strain accumulation. Annealing after roughing rolling simulation led to the nucleation of fine grains in the Control, which suggests that delaying finishing rolling would promote recrystallization and the breakdown of the cast structure.

Keywords dynamic recrystallization, electron backscatter diffraction, ferritic stainless steel, finishing, roughing

1. Introduction

Ferritic stainless steels (FSS) have sparked interest among researchers in recent times (Ref 1-5). Aside from grain refinement through controlling inclusions during solidification (Ref 6), the austenite-ferrite phase transformation is beneficial in texture randomization, which leads to the reduction of plastic anisotropy of steels. Unfortunately, the 436 grade of stainless steel does not undergo such a phase transformation (Ref 4). This poses difficulty in breaking down texture build up, as the only viable means for texture randomization is through recrystallization.

For FSSs, the cast columnar structure tends to exhibit the cube texture orientations, which is known to be difficult to recrystallize due to the low Taylor factor (Ref 7). The low Taylor factor coupled with high stacking fault energy (SFE) perpetuate the cube texture in subsequent hot rolling processes resulting in grain anisotropy and finally ridging (Ref 3). Ridging occurs where bands of preferred orientations align along the rolling direction, resulting in non-uniform deformation during drawing of rolled products. This is unsatisfactory for product quality and requires polishing to improve the final material finish (Ref 2, 8). It has been established that preferred orientations that align to the rolling direction in the final rolled sheet is a result of upstream processes from casting, hot rolling and cold rolling and as such, the entire process has to be optimized and considered during research (Ref 3).

During deformation of metals, energy is stored within the material in the form of dislocations also referred to as retained strain. These areas of high misorientation act as a driving force for recovery or recrystallization (Ref 9, 10). Recovery and recrystallization are competing restoration mechanisms, with recovery being the dominant restoration mechanism in high SFE materials such as FSS. Recrystallization when known to occur during the deformation process is referred to as dynamic recrystallization.

The need to encourage recrystallization over recovery in FSS, requires that the internal energy or retained strain be increased (Ref 11). As mentioned earlier, this is a challenge as recovery tends to reduce the retained strain, thereby limiting the driving force for recrystallization. Many authors have attempted to work around this by increasing the retained strain during hot deformation. Mehtonen et al. (Ref 12) found that work hardening was improved under higher Zener-Hollomon parameters as recovery was favored, while low Zener-Hollomon parameters favored recrystallization of new grains through continuous dynamic recrystallization (CDRX). Most recently, Kisko et al. (Ref 13) among many others (Ref 1, 14) looked into lowering the finishing rolling temperature ranges. Although lowering deformation temperature during hot rolling improved the recrystallization, low finishing rolling temperatures result in higher mill roads, excessive wear of rolls,

Muhammed Salojee, Charles W. Siyasiya, and **Kofi A. Annan**, Department of Materials Science and Metallurgical Engineering, University of Pretoria, Private bag X20, Hatfield, Pretoria 0002, South Africa; and **Joseph S. Moema**, Mintek, Physical Metallurgy Group, Private bag X20, Randburg, Gauteng, South Africa. Contact e-mails: u13271050@tuks.co.za, charles.siyasiya@up.ac.za, kofi.annan@up.ac.za, and josephm@mintek.co.za.

tripping off of rolling mill and ultimately reduced operational efficiency which adds to cost of production. Cho et al. (Ref 15] looked into variations in retained strain through alternate reduction sequences in FSSs' restoration behavior. The first process route had a 67% reduction followed by a 50% reduction, and the alternate route having a 50% height reduction followed by a 67% reduction. They found that alternating the reduction sequence had no significant influence on grain size and texture; however the latter process route produced a sharper γ-fibre texture. This suggests that delaying strain retention in later stages could improve ridging resistance in FSSs. Lui et al. (Ref 16) found that higher deformations increased nucleation sites and increased retained strain which resulted in finer grain size. However, not many authors focused on the retaining strain during hot rolling to enhance the recrystallization process, thereby reducing or eliminating the effects of ridging. The following research sought to understand the microstructural effect of retaining strain during roughing rolling through increased inter-pass time and strain on the final finishing rolling product of 436 FSS.

2. Material and Methods

The studied, niobium (Nb) stabilized, 436 FSS was received in as-cast condition and was supplied by Columbus Stainless. The composition of the steel in mass.%, was as follows: 0.014C-0.39Mn-0.42Si-0.27Ni-17.2Cr-1.22Mo-0.415Nb. Samples were wire-cut into cylindrical shapes of 15 mm length and 10 mm diameter from the columnar region of the slab. The microstructure of the columnar grains present is found in Fig. 1.

These samples were deformed in a Gleeble 1500 in six-passes under uniaxial, axisymmetric, isothermal, compression tests normal to the direction of the cast. The deformation parameters are contained in Table 1. Out of the six-passes, the first three-passes were used to simulate roughing and the last three-passes simulated finishing rolling. Samples were heated to 1080 °C at 20 °C/s and soaked for 300 s. Strain rates were limited to 5/s. The first test series was designed to simulate the industry deformation condition as a benchmark. In the second and third series, the inter-pass times (INT) and, inter-pass time plus strain (INT + S) were increased, respectively. The samples were quenched in helium (He) to freeze the microstructures at pass three (P3) and six (P6).

The samples were sectioned parallel to the deformation axis through the center to avoid the dead zone, as shown in Fig. 2.

Samples were ground to a 2400-grit and polished to 1 μm finish for optical microscopy (OM). The SEM-EBSD samples were subsequently electropolished using A3® solution for 20 s at 23 V to remove the deformed layer. The specimens were analyzed at a working distance of 20 mm with an accelerating voltage of 20 kV and a tilt angle of 70°. The SEM-EBSD scanning step size was 0.5 μm. Vickers microhardness measurements were performed using an automated Duramin hardness indenter to characterise the extent of softening after hot deformation. With further EBSD carried out on the Control and INT + S simulations after annealing at 800 °C for 600 s for both roughing and finishing simulations.

3. Results and Discussion

Figure 3 shows the von Mises stress-equivalent strain graphs after roughing rolling simulations outlined in Table 1. As may be seen, all deformation schedules showed increased flow stress with applied strain for the first three-passes; this is typical of strain hardening behavior observed by previous authors (Ref 17, 18). The Control and INT deformation schedules show that both the second and third passes continued along the prior deformation path, however the INT + S schedule did not. This was attributed to recovery in the latter due to longer inter-pass time compared to the Control sample. In other words, Control and INT experienced more work hardening as a result of shorter inter-pass and, therefore, less recovery, Fig. 4.

Inverse pole figure (IPF) maps with the associated local misorientation maps are given in Fig. 4. Local misorientation maps calculate the average misorientation of each pixel relative to its surrounding pixels and assigns the average misorientation to it. Misorientations above 5° are discarded, so as to exclude grain boundaries in calculations of strain. It is clear from the misorientation maps that Control and INT schedules exhibited more retained strain as revealed by a high fraction of substructure. On the contrary, the INT + S schedule underwent more recovery due to the increased strain and inter-pass time. This was attributed to the increased strain in pass 1 leading to

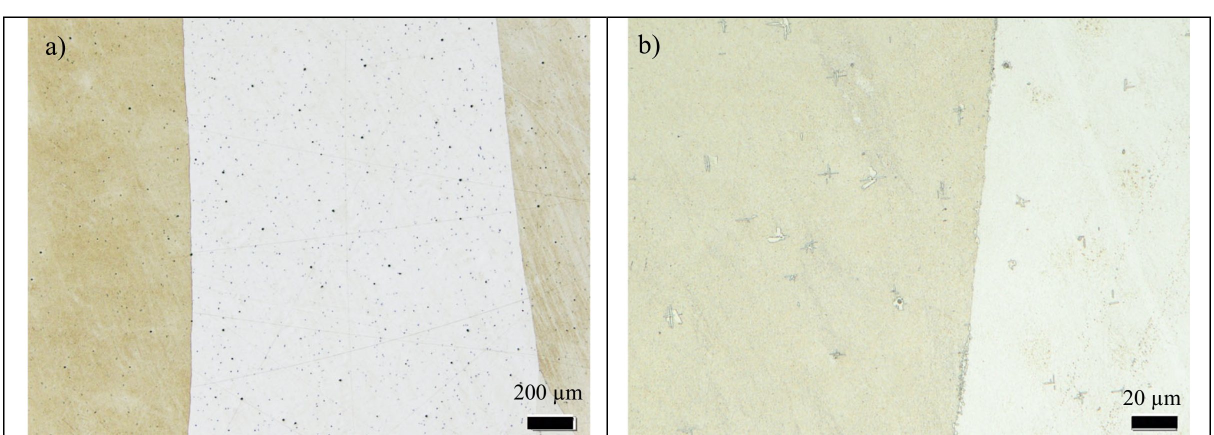

Fig. 1 As-cast microstructure taken at (a) 50X and (b) 500X magnification along the transverse plane of the columnar region

Table 1 Parameters for the hot rolling simulations

Experimental	Parameter	Roughing			Finishing		
		P1	P2	P3	P4	P5	P6
	Temperature (°C)	1000	950	930	920	915	910
Control	Inter-pass (s)	11	14	18,3	36	38	52
	Strain	0.18	0.20	0.3	0.20	0.20	0.20
Simulation 1 (INT)	Inter-pass (s)	15	20	25	36	38	52
	Strain	0.18	0.20	0.3	0.20	0.20	0.20
Simulation 2 (INT + S)	Inter-pass (s)	15	20	25	36	38	52
	Strain	0.20	0.3	0.3	0.20	0.20	0.20

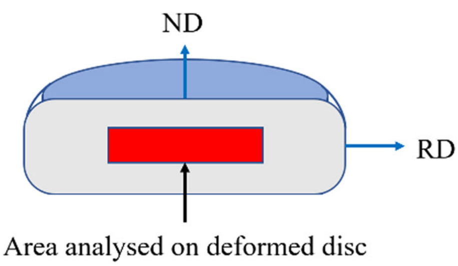

Fig. 2 Deformed area of interest with corresponding area analyzed highlighted in red to avoid dead zones

more retained strain in pass 2, which triggered static restoration in the form of recovery during the inter-pass time between passes 2 and 3, the retained strain was not sufficient to trigger recrystallization over recovery as explained by Cai et al (Ref 11).

Stabilized FSSs like 436 contained particles which are responsible for particle stimulated nucleation (PSN) of new grains around the particles due to strain localization. PSN is well known to promoting texture randomization through dynamic recrystallization (Ref 9, 10, 19). Contrary to Control and INT schedules, INT + S schedule did not show substantial strain concentration around particles compared to the Control and INT schedules, Fig. 4. This was attributed to the longer inter-pass times which in turn resulted in less PSN.

Figure 5 shows the six-pass deformation curves for the three schedules. After pass 3, the softening between passes was more significant with each successive pass although the temperature was not significantly varied, Table 1, similar findings were produced by Pussegoda et al. (Ref 20), where they attribute such behavior to DDRX. In other words, the maximum stress decreased with each successive pass, which signified substantial fraction of either dynamic, static or both restoration mechanisms at play. Due to smaller strains per pass, i.e., an average of 0.2 strain, the flow stresses never reached steady state, and as such, it cannot be deduced whether dynamic restoration had been completed or not.

Figure 6 shows that the restoration mechanism was largely recovery as evidenced by the few solid black lines which represent HAGBs. This essentially means that restoration was not sufficient to break down the as-cast structure this is a known concern similar to work produced by Ma et al. (Ref 21). As opposed to the three-pass roughing rolling simulation, the six-pass roughing and finishing rolling simulation exhibited a well-defined sub-grain boundary network, typically evidence of the onset and progression of CDRX (Ref 19).

The Control and INT schedules with the associated strain after three-passes, would have had a high driving force for recovery during the higher temperature associated with early stages of finishing due to the high retained strain. The INT + S schedule however, underwent recovery earlier on during roughing, correlating to work by Mehtonen et al. (Ref 12). Recovery lowers retained strain to a lower extent as opposed to recrystallization (Ref 10, 19); therefore, the INT + S schedule entering finishing rolling did not reach the critical strain for recrystallization as evident in Fig. 6. The microstructure looks largely recovered and as such it can be suggested that the microstructure was driven to recovery in those schedules. The INT + S schedule recovered to an extent after roughing, allowing strain accumulation during finishing by preventing premature recovery. However, the Control and the INT schedules had initiated restoration during finishing.

All simulation schedules in general, failed to break down the inherent cube texture of the continuously cast slabs. The sub-grain structure was still prevalent even after six-passes, Fig. 6, with the general orientation, being aligned to the parent grain as hot rolling does not have as strong an influence on breaking down the as-cast texture as cold rolling (Ref 21). Therefore, it can be deduced that although restoration occurred to a limited extent, the restoration mechanism was largely dynamic and static recovery for the areas observed.

Figure 7 shows the correlated misorientation angle distributions (MADs) for three and six-pass schedules for the maps presented in Fig. 4 and 6. Correlated MADs essentially show the general misorientation between neighboring points. As may be seen from Fig. 7, the roughing rolling simulation yielded larger high angle grain boundaries (HAGBs) densities. The high degree of low angle grain boundaries (LAGBs) is typical of the onset of CDRX.

From roughing to finishing rolling simulation, the LAGB frequencies increased in all schedules, denoted the onset and progression of CDRX, which is common in high SFE materials such as FSSs. The formation of LAGBs is also evident in Fig. 4 and 6, where sub-grain structure is evident especially after finishing rolling simulations. Although the structure showed a well-defined sub-grain structure after six-passes, IPF maps showed minimal changes in orientations relative to the parent grain.

To ascertain the extent of retained strain after three and six-pass deformations, hardness tests were undertaken, before and after annealing at 800 °C for 600 s, Table 2. The results showed that the INT + S, with increased strain per pass in the initial passes and increased inter-pass time softened to a far

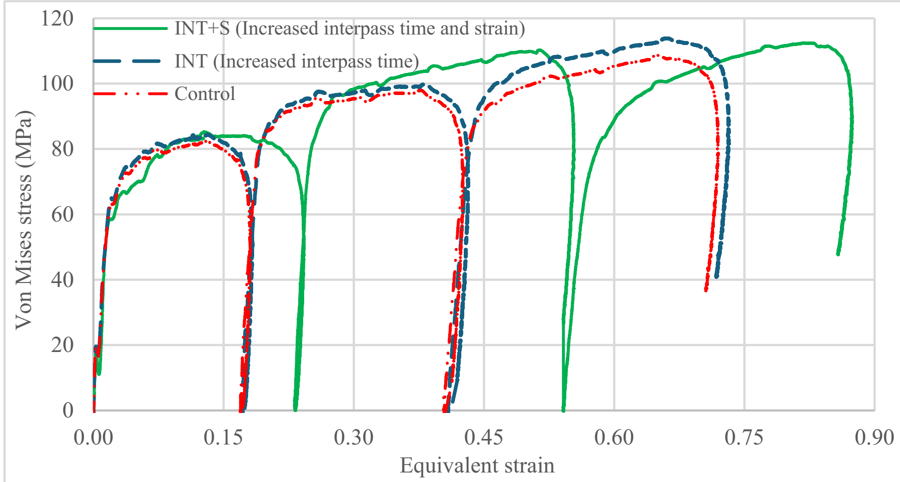

Fig. 3 Flow stress curves for three-pass roughing rolling simulation carried out under different roughing conditions at 5/s, more details provided in Table 1. Control defines close to industrial conditions, INT, increased inter-pass times and INT + S, increased inter-pass times and strain

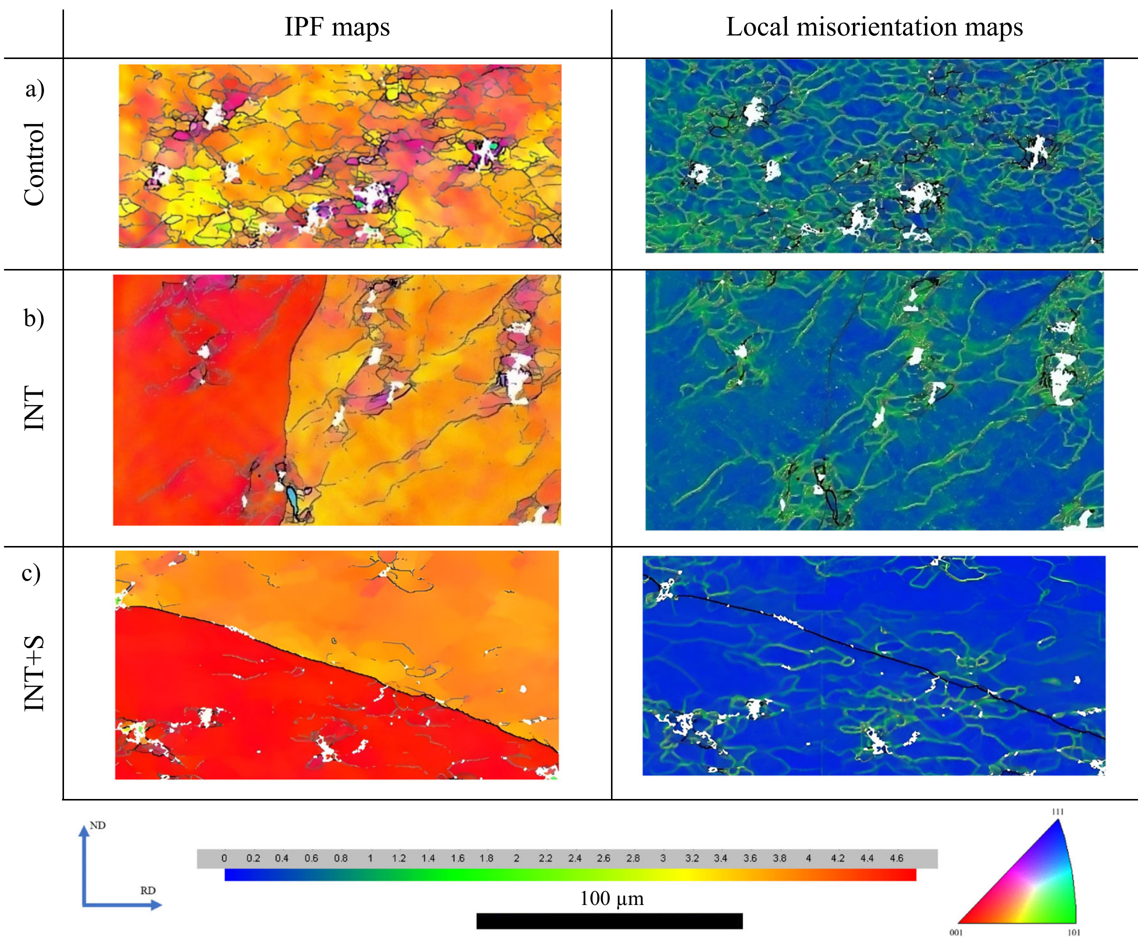

Fig. 4 Variations in IPF figures after three-passes with associated local misorientation plots for roughing simulations in the, (a) Control, (b) INT and (c) INT + S roughing rolling simulations after pass 3, taken at a 0.5-μm step size. Gray lines define boundaries with misorientations below 15°, and black lines, for boundaries greater than 15°. Areas in white are unindexed, generally associated with precipitates or inclusions

greater extent (14%) than the rest after six-passes. This was attributed to the least restoration after deformation, Table 2.

Figure 8 shows the recrystallization maps of three and six-pass schedules before and after annealing of the Control and INT + S, i.e., the two extreme results. The processing of

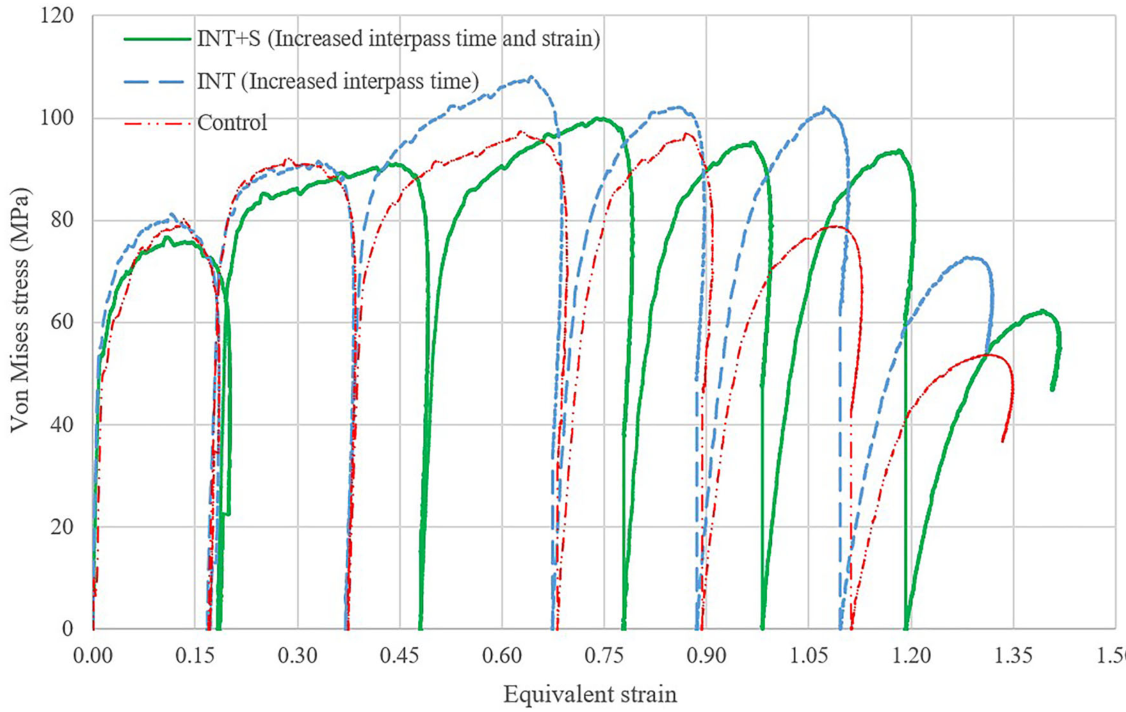

Fig. 5 True stress-strain graphs for six-pass schedules from roughing and finishing rolling simulations, Control and INT, had an increase in inter-pass time in the first three-passes and INT + S had an increase in inter-pass time and strain in the first three-passes

recrystallization maps was done using Channel 5 software, where grains are reconstructed and if the average misorientation within a grain exceeds 1° misorientation then a grain is defined to be deformed and assigned a red color. When the average misorientation in a grain does not exceed 1° misorientation but has a misorientation between sub-grains exceeding 1°, they are classified as substructure and assigned a yellow color. All remaining grains are seen to have minimal deformation, are deemed recrystallized and assigned the color blue.

As may be seen from Fig. 8, the Control exhibited the largest amount of restoration after finishing but before annealing, manifested in the increased fraction of recrystallized grains. On the contrary, before annealing, the INT + S showed less recrystallization after both three and six-passes than the former, i.e., the material was mostly substructure, Table 3. Furthermore, it can be seen that finer grains nucleated after annealing the Control after roughing due to the highly deformed structure, in red. This suggests that these fine grains can potentially act as nucleation sites for DDRX, and therefore, drive recrystallization during hot working (Ref 9, 10, 19). In other words, these fine grains can increase the likelihood of either DDRX or CRDX during finishing rolling, that is, if the finishing rolling is delayed after exiting the roughing rolling to allow for SRX. Noteworthy is the observation that annealing after six-pass for both schedules as well as INT + S-roughing, the microstructures were found to be more or less the same, i.e., coarser and less recrystallized grains, which suggest less driving force for SRX. The evolution of the microstructures was quantified using SEM-EBSD and is summarized in Table 3.

In general, laboratory simulations are not an adequate representation of plant scale testing. The three-passes in this study were applied to simulate roughing rolling with an additional three-passes simulating finishing rolling. The typical industrial reverse roughing rolling and Steckel mill finishing rolling takes about 7-passes each with strains per pass ranging from 0.17 to 0.24 resulting in about 1.6 total strain. The strain rates in the plant can range from 4 to 20/s during roughing and from 20 to 100/s during finishing which is substantially higher than the laboratory strain rates of 5 /s used in this work. It is known that higher strain rates encourage strain accumulation during rolling (Ref 22) which would aid in recrystallization; therefore the study is expected to depict worst case scenario conditions, while plant scale trials are likely to improve results substantially.

Retained strain on an industrial scale mentioned would have higher potential to drive recrystallization forward through the INT + S following finishing rolling simulation in this study. Retained strain, specifically at lower temperatures (Ref 1, 18), holds the potential for DDRX to occur and as a result the potential for texture randomization which was not achieved in this study. Overall, the process proposed would promote restoration through recovery at higher temperatures and facilitate recrystallization during finishing.

From this study, particularly from the annealed Control schedule after roughing, evidence points to the presence of a fine-grained structure. Fine-grained structures have been found to favor recrystallization during hot rolling (Ref 23). The concept of intermediate annealing has generally been studied among researchers during cold rolling (Ref 4, 24), but has not been delved into in terms of hot rolling simulations. These results suggest that delaying finishing rolling after roughing rolling could be beneficial by promoting recrystallization before entering the finishing rolling mill (Ref 25-33).

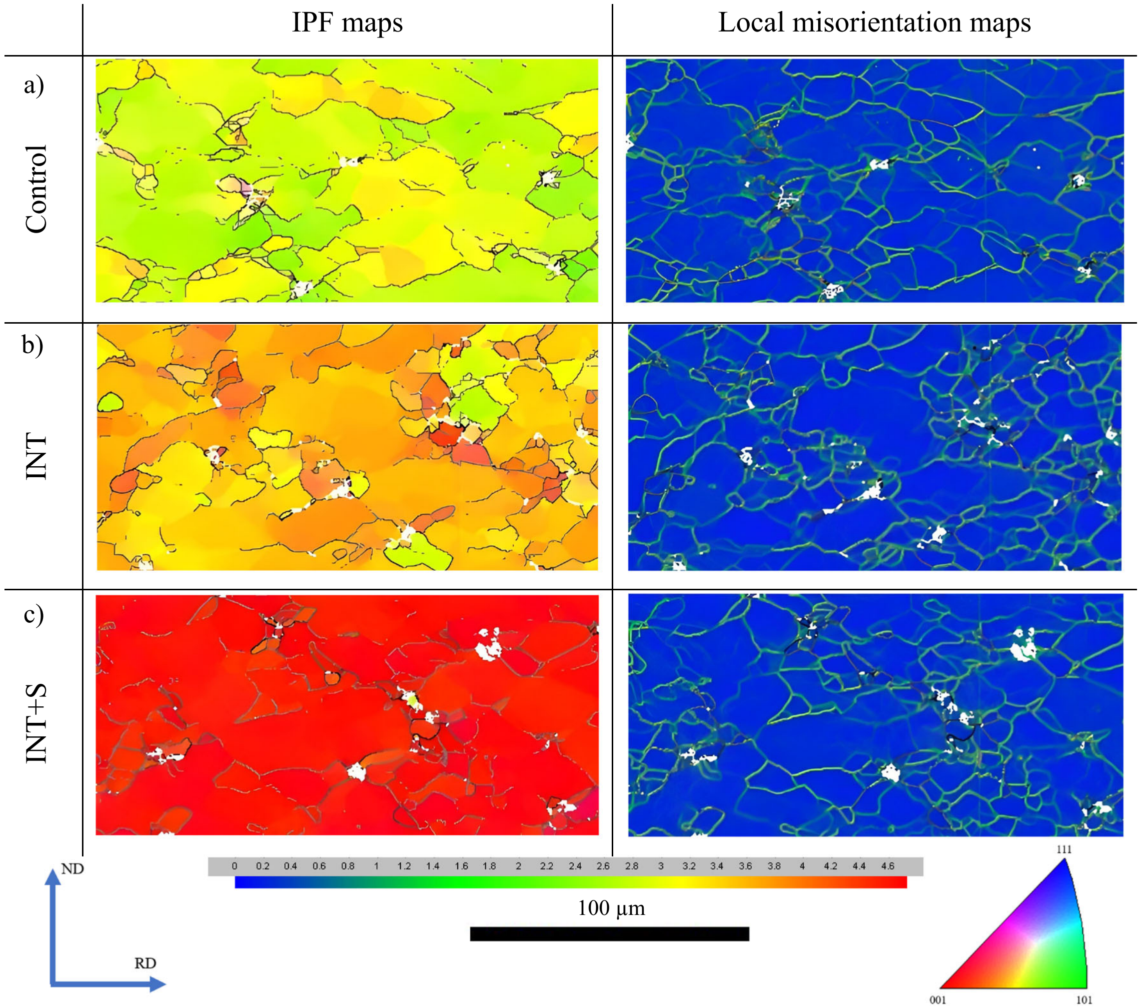

Fig. 6 Variations in IPF figures after three and six-passes with associated local misorientation plots for (a) Control, (b) INT and (c) INT + S rolling simulations, with associated. Maps taken at a 0.5-μm step size, all samples are observed at the same magnification. Gray lines define boundaries with misorientations below 15°, and black lines, for boundaries greater than 15°. Areas in white are unindexed, typical of precipitates or inclusions

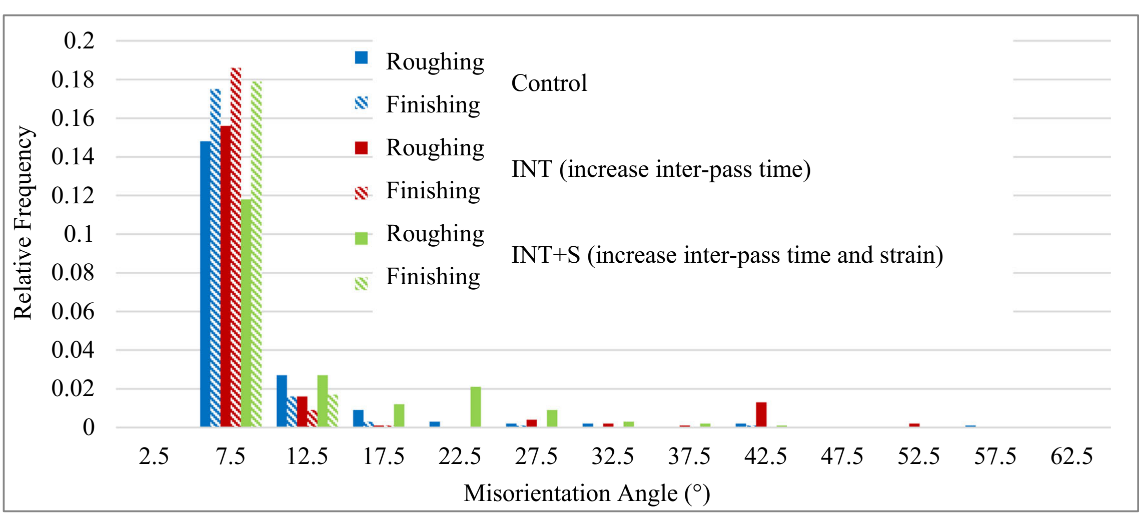

Fig. 7 Correlated misorientation data for three and six-pass deformation schedules for the IPF maps contained in Fig. 4 and 6

Table 2 Average hardness results before and after annealing

	Three-pass			Six-pass		
	Before anneal	After anneal	ΔHV (%)	Before anneal	After anneal	ΔHV (%)
Control	171.5 ± 2.6	167.6 ± 4.8	-3.0 (2.2)	160.8 ± 3.6	157.6 ± 3.3	-3.2 (2.0)
INT	173.0 ± 3.5	159.0 ± 1.4	-19.9 (11.1)	168.5 ± 1.2	156.1 ± 1.7	-12.4 (7.4)
INT + S	172.2 ± 3.5	161.9 ± 4.1	-10.3 (6)	192.6 ± 3.3	165.3 ± 4.4	-27.3 (14.2)

The negative ΔHV (%) values denote a decrease in hardness due to static recrystallization (SRX) and the percentage change in parenthesis

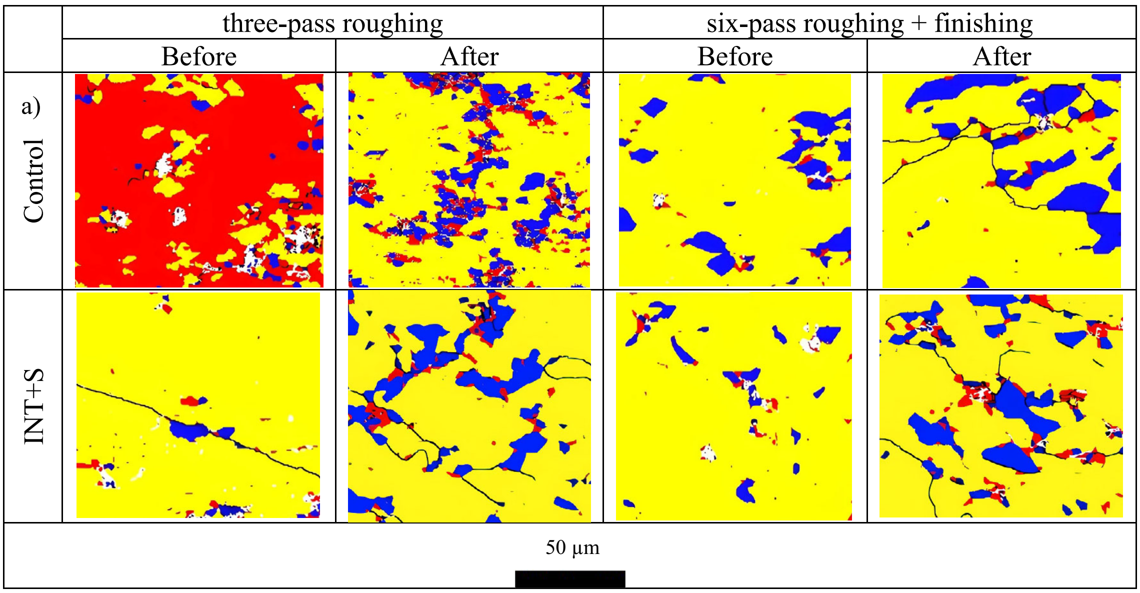

Fig. 8 Variations in (a) The Control and (b) the INT + S recrystallization maps after three and six-passes, before and after annealing at 800 °C for 600 s. All samples are observed at the same magnification. Black lines represent boundaries greater than 15°. Red areas represent deformed material, yellow represents substructure material, and blue represents recrystallized material (Color figure online)

Table 3 Recrystallization percentage data after three and six-passes for recrystallization maps before and after annealing in Fig. 8

		Roughing		Finishing	
		Before	After	Before	After
Control	Recrystallized	3.0	15.6	8.9	14.3
	Substructure	37.2	73.3	88.7	83.4
	Deformed	59.7	11.1	2.4	2.3
INT + S	Recrystallized	2.6	12.5	2.6	8.7
	Substructure	95.2	84.9	96.3	88.0
	Deformed	2.2	2.6	1.1	3.3

4. Conclusion

The effects of strain and inter-pass time on the restoration behavior of 436 ferritic stainless steel were investigated via three-pass roughing and three-pass finishing rolling simulations using the Gleeble 1500 thermomechanical processing simulator. The Control, which is the industry benchmark, showed more recrystallization after roughing rolling simulation and annealing. Similarly, it also showed more recrystallization after simulated finishing and annealing. Which implies that if the finishing rolling is delayed to allow for static recrystallization, more recrystallization can be realised after finishing rolling and annealing. On the contrary to the expectation, the increased inter-pass time and strain INT + S schedule resulted in less recrystallization even after simulated finishing rolling and annealing. This was attributed to limited amount of strain and strain rate imposed on the steel under the laboratory rolling conditions. However, the increased inter-pass time and strain might yield different results under full scale plant trial.

Acknowledgements

The authors are grateful for the technical assistance from IMMRI, research facilities from the University of Pretoria and the financial and technical support from Columbus Stainless Pty Ltd and Mintek.

Funding

Open access funding provided by University of Pretoria.

References

1. F.V. Braga, Hot Deformation Behavior of a Ferritic Stainless Steel Stabilized with Nb During Hot Rolling Simulation at Different Temperature Ranges, *J. Mater. Res.*, 2016, **31**(5), p 635–645
2. G. Lefebvre, Relationship Between Microstructure, Texture and Ridging in Ferritic Stainless Steels. University of British Columbia, Materials Engineering, Vancouver, 2014
3. P. Modak, S. Patra, R. Mitra, and D. Chakrabarti, Effect of Starting As-Cast Structure on the Microstructure-Texture Evolution During Subsequent Processing and Finally Ridging Behavior of Ferritic Stainless Steel, *Metall. Mater. Trans. A Phys. Metall. Mater. Sci.*, 2018, **49**(A), p 2219–2234
4. H.J. Uananisa, C.W. Siyasiya, W.E. Stumpf, and M.J. Papo, The Influence of Thermomechanical Processing on the Surface Quality of an AISI 436 Ferritic Stainless Steel, *J. South. Afr. Inst. Min. Metall.*, 2016, **116**, p 981–986
5. X. Ma, J. Zhao, W. Du, X. Zhang, L. Jiang, and Z. Jiang, Quantification of Texture-Induced Ridging in Ferritic Stainless Steels 430 and 430LR During Tensile Deformation, *J. Mater. Res. Technol.*, 2019, **8**(2), p 2041–2051
6. S. Kondokula, *Thesis: Ridging of Stabilised Ferritic Stainless Steels-The Effects of Casting and Hot-Rolling Parameter*, University of Oulu-Faculty of Technology, Finland, 2021
7. S. Lee and B.C. de Cooman, Effect of Warm Rolling on the Rolling and Recrystallization Textures of Non-Oriented 3% Si Steel, *ISIJ Int.*, 2011, **51**(9), p 1545–1552
8. O. Engler and V. Randle, *Introduction to Texture Analyis: Macrotexture, Microtexture and Orientation*, 2nd ed. CRC Press, New York, 2010
9. F.J. Humphreys and M. Hatherly, *Recrystallization and Related Annealing Phenomenon*, 2nd ed. Elsevier, Oxord, 2004
10. D. Raabe, Recovery and Recrystallization: Phenomenon, Physics, Models, Simulations. in *Physical Metallurgy*, Germany, Elsevier, 2014, pp. 2291-2396
11. G. Cai, C. Li, D. Wang, and Y. Zhou, Texture Evolution of Annealed Fe-19Cr-2Mo-Nb-Ti Ferritic Stainless Steel. in 17th International Conference on Metal Forming, Procedia Manufacturing, Toyohashi, 2018
12. S.V. Mehtonen, L.P. Karjalainen, and D. Porter, Hot Deformation Behavior and Microstructure Evolution of a Stabilized High-Cr Ferritic Stainless Steel, *Mater. Sci. Eng. A*, 2013, **571**, p 1–12
13. A. Kisko, A. Kaijalainen, L. Kurtti, S. Kodukula, and T. Ylimäinen, The Effect of Hot Rolling and Coiling Temperature on Microstructure and Texture of Ferritic Stainless Steel. *La Metallurgia Italiana,* no. July-August, pp. 16-23, 2022
14. S. Kodukula, H. Kokkomäki, E. Puukko, D. Porter, and J. Kömi, Influence of Hot Rolling Finishing Temperature on Texture and Ridging Resistance in Stabilized Ferritic Stainless Steel, *Steel Res. Int.*, 2021, **92**, p 1–11
15. S.H. Cho, Y.J. Lee, W. Bahanan, J.M. Oh, D.-J. Kim, J.-H. Kang, J. Ryu, P. Widiantara, and Y.G. Ko, Effect of Reduction Sequence During Rolling on Deformed Texture and Anisotropy of Ferritic Stainless Steel, *Materials*, 2023, **16**(3767), p 1–11
16. H. Liu, H. Li, C. Liu, and J. Wu, Effect of Rolling Reduction on Microstructure and Formability of a Ferritic Stainless Steel, *J. Mater. Eng. Perform.*, 2024, **33**(3), p 1304–1313
17. F.V. Braga, D.P. Escobarb, T.J.Á. Reis, N.JLd. Oliveira, and M.S. Andrade, Recrystallization of Niobium Stabilized Ferritic Stainless Steel During Hot Rolling Simulation by Torsion Tests, *J. Mater. Res. Technol.*, 2016, **5**(1), p 92–99
18. S. Mehtonen, E. Palmiere, D. Misra, P. Karjalainen, and D. Porter, Microstructural and Texture Development During Multi-pass Hot Deformation of a Stabilized High-Chromium Ferritic Stainless Steel, *ISIJ Int.*, 2014, **54**(6), p 1406–1415
19. K. Huang and R. Logé, A Review of Dynamic Recrystallization Phenomena in Metallic Materials, *Mater. Des.*, 2016, **111**, p 548–574
20. L.N. Pusseoda, S. Yue, and J.J. Jonas, Laboratory Simulation of Seamless Tube Piercing and Rolling Using Dynamic Recrystallization Schedules, *Metall. Trans.*, 1990, **21**(A), p 153–164
21. X. Ma, J. Zhao, W. Dub, X. Zhang, and Z. Jiang, Effects of Rolling Processes on Ridging Generation of Ferritic Stainless Steel, *Mater Charact*, 2018, **137**, p 201–211
22. C. Zhang, Z. Liu, and G. Wang, Effects of Hot Rolled Shear Bands on Formability and Surface Ridging of an Ultra Purified 21%Cr Ferritic Stainless Steel, *J. Mater. Process. Technol.*, 2011, **211**, p 1051–1059
23. J. T. Asante and S. C. W., "Evolution of Microstructures in High and Low Ti/Al Ratio Ferritic Stainless Steels after Hot Rolling. in MATEC Web of Conferences 388, 2023 RAPDASA-RobMech-PRASA-AMI Conference, 2023
24. D.G. Rodrigues, C.M. Alcântara and TRd. Oliveira, Evaluation of Intermediate Annealing on Nb-Stabilized Ferritic Stainless Steel, *Mater. Res.*, 2017, **20**, p 298–303
25. Damstahl, Brochure. in *Technical Information*, Damstahl, Ed., Skanderborg, Damstahl, 2015, pp. 250-285
26. Columbus Stainless Steel Pty Ltd, "Dowloads/Technical Brochures," 15 July 2020. [Online]. Available: https://www.columbus.co.za/
27. K. A. Annan. Effect of Hot Working Characteristics on the Texture Development in AISI 430 and 433 Ferritic Stainless Steel. University of Pretoria, Department of Materials Science and Metallurgical Engineering, Pretoria, 2012
28. H.C. Chao, Recent Studies into the Mechanism of Ridgin in Ferritic Stainless Steels, *Metallurg. Trans.*, 1971, **4**, p 1973–1183
29. H. Takechi, H. Kato, T. Sunami, and T. Nakayama, The Mechanism of Ridging Formation in 17% Chromium Stainless Steel Sheets, *Trans. Japan Inst. Met.*, 1967, **8**, p 233–239
30. M. G. Maruma. Effect of Composition and Thermomechanical Processing on Texture Evolution, Formability and Ridging Behaviour of Ferritic Stainless Steel. Department of Materials Science and Metallurgical Engineering, University of Pretoria, Pretoria, 2013
31. S. Mehtonen, *The Behavior of Stabilized High-Chromium Ferritic Stainless Steels in Hot Defromation*, Acta Universitatis Ouluensis, Oulu, 2014
32. G.K. Mandal, S.S. Das, T. Kumar, A. Kamaraj, K. Mondal, and V.C. Srivastava, The Role of Precipitates in Recrystallization Mechanism of Nb-Mo Microalloyed Steel, *J. Mater. Eng. Perform.*, 2018, **27**, p 6748–6757
33. F. Gao, Z. Liu, H. Liu, and G. Wang, Texture Evolution and Formability Under Different Hot Rolling Conditions in Ultra Purified 17%Cr Ferritic Stainless Steels, *Mater Charact*, 2023, **75**, p 93–100